Langmuir

Article

pubs.acs.org/Langmuir

Polyhedral Oligomeric Silsesquioxane-F68 Hybrid Vesicles for Folate Receptor Targeted Anti-Cancer Drug Delivery

Bindu P. Nair, Dhanesh Vaikkath, and Prabha D. Nair*

Division of Tissue Engineering and Regeneration Technologies, Biomedical Technology Wing, Sree Chitra Tirunal Institute for Medical Sciences and Technology, Thiruvananthapuram 695012, Kerala, India

Supporting Information

ABSTRACT: Polyhedral Oligomeric Silsesquioxane (POSS)-F68 hybrid vesicles with an average diameter of 700 nm are produced using a stable solution of heterofunctional POSS having 3-aminopropyl and vinyl groups and pluronic F68 in ethanol−water mixture. Thermogram and zeta potential values evidence the spontaneous self-assembly of POSS into bilayers through H-bonding interaction between the aminopropyl groups, and the effective stabilization of the POSS-bilayers by amphiphilic F68 during solvent-evaporation to form the vesicles. The vesicles are noncytotoxic and dispersible in aqueous solvents through steric stabilization provided by the hydrophilic F68. A highly facile coinclusion method has been used for making doxorubicin and folic acid loaded vesicles. Doxorubicin loaded in the vesicles exhibits a controlled release profile in phosphate buffered saline. Confocal microscopic and flow cytometric studies on the endocytosis of the vesicles by HeLa and HOS cells prove that a noncovalent entrapment of excess folic acid in the vesicles through H-bonding is sufficient to enhance the uptake significantly. POSS-F68 vesicles in combination with folic acid and a chemotherapeutic can have potential for targeted intracellular anti-cancer drug delivery.

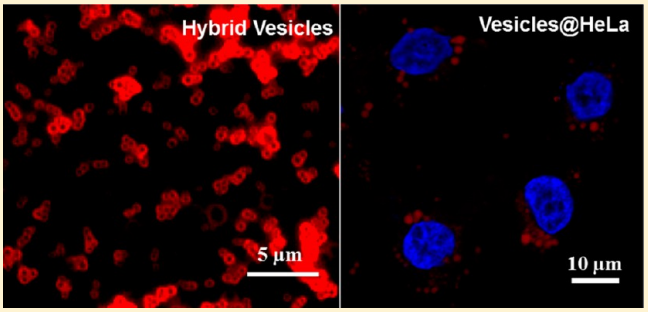

1. INTRODUCTION

Targeted drug delivery to specific malfunctioning cell populations of cancer sites is an active area of research today as most of the anti-cancer drugs cause serious side effects on healthy noncancerous cells.[1−3] Cellular targeting is usually achieved by using antibodies or ligands to target receptors expressed specifically by the cancer cells. Use of folic acid as a targeting ligand has emerged as a facile strategy in recent years because most of the cancer cells such as ovarian, cervical, breast, lung, renal, and neuroendocrine carcinoma overexpress folate receptor when compared to other normal cells.[4−8]

Among various materials useful for fabricating drug carriers, shape persistence and longer degradation time of silica make them highly attractive when compared to polymers and surfactants.[9−12] Another advantage of silica is the tunability of its porosity and pore size during synthesis through a careful choice of functional group interaction, which facilitates a high cargo of drug molecules being carried in it. Therefore, various siliceous morphologies have been extensively studied for targeted drug delivery and imaging applications in recent years.[13−17] Pure siliceous or silica−organic hybrid vesicles can be of particular interest in cancer therapy as vesicles can improve treatment efficacy of anti-cancer drugs due to enhanced permeability and retention properties.[18]

POSS is the smallest and precisely defined silica nanoparticle having the general formula $(RSiO_{1.5})_8$, which contains a polyhedron silicon−oxygen cube skeleton with intermittent siloxane linkages and tunable organic groups at the silicon atoms. POSS has been studied for drug delivery applications,[19−21] and POSS-hybrid morphologies have been fabricated through self-assembly induced by polymer or surfactant chains covalently attached to the POSS core.[22−26] More recently, POSS-hybrid vesicles of diameter in the range of 2−4 μm were fabricated through thiol−ene photopolymerization in toluene−water mixture.[27] However, fabrication of stable POSS-hybrid vesicles through self-assembly and noncovalent stabilization is not reported hitherto in the literature. In this Article, we report the fabrication of stable POSS-F68 hybrid vesicles with an average diameter of 700 nm through a single-step self-assembly method. F68 is a U.S. Food and Drug Administration (FDA) approved pluronic poly(ethylene oxide) (PEO)−poly(propylene oxide) (PPO)−(PEO) triblock copolymer. It has been proven that pluronics are effective in the treatment of drug-resistant tumors.[28] The vesicles thus obtained have the advantage of shape persistence due to inorganic POSS and dispersibility in aqueous medium through steric stabilization of hydrophilic F68. The method is also highly facile with minimum functionalization and purification steps, and a highly achievable loading efficiency due to the solvent evaporation technique used. The structural aspects and

Received: September 24, 2013
Revised: November 26, 2013
Published: December 19, 2013

   dx.doi.org/10.1021/la4036997 | Langmuir 2014, 30, 340−347

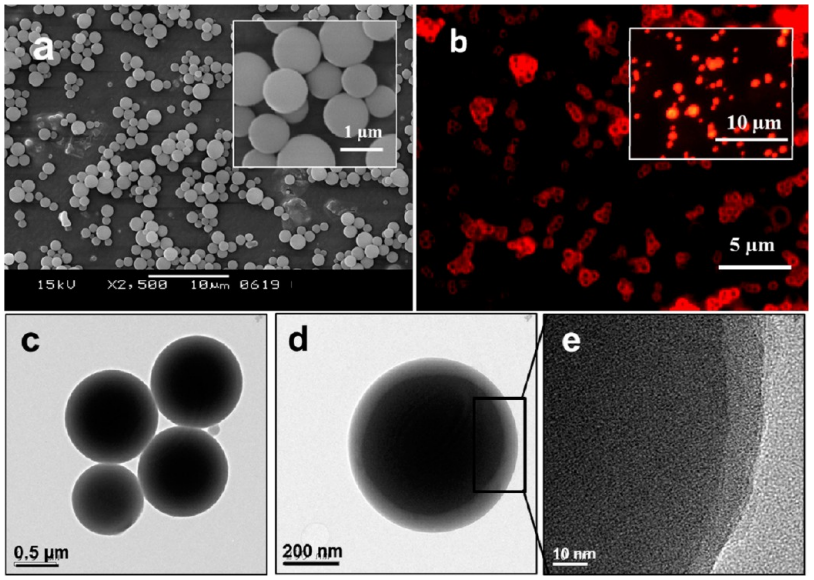

Figure 1. (a) SEM, (b) fluorescent micrograph, (c and d) TEM, and (e) HR-TEM of POSS-F68 vesicles.

the in vitro evaluation of the POSS-F68 vesicles for controlled drug delivery applications are illustrated using chemotherapeutic doxorubicin. We also demonstrate the folate receptor targeting capacity of the POSS-F68 vesicles through a simple noncovalent conjugation of folic acid.

2. MATERIALS AND METHODS

2.1. Materials. 3-Aminopropyltriethoxysilane (99%, AS) and vinyltriethoxysilane (97%, VS), F68, 3-(4,5-dimethylthiazol-2-yl)-2,5-diphenyl tetrazolium bromide (MTT), folic acid (FOL), and doxorubicin hydrochloride (DOX) were purchased from Aldrich Chemicals, and absolute ethanol (spectroscopic grade) was from S. D. Fine Chem. Limited, India. Millipore-grade water was used. Dulbecco's Modified Eagles Medium (DMEM, High Glucose), fetal bovine serum (FBS), and penicillin-streptomycin were procured from Gibco (U.S.). Mouse fibroblast cell line (L929), human cervical cancer cell line (HeLa), and human osteosarcoma cell line (HOS) were subcultured from a stock culture obtained from the National Centre for Cell Sciences, India.

2.2. Fabrication of POSS-F68 Vesicles. POSS solution from AS/VS composition was prepared by following the procedure reported elsewhere.[29] Typically, hydrolytic co-condensation was carried out by diluting a mix of AS and VS with an AS:VS mole ratio of 1:3 using ethanol−water mixture (v/v = 14/1) to a silane concentration of 0.45 M and aging the solution in a closed container at ambient temperature for a period over 7 days. The clear and transparent POSS solution thus obtained was then diluted with absolute ethanol in a 1:10 ratio and mixed with F68 at a POSS:F68 weight ratio of 1:1. The POSS:F68 solution thus obtained was cast on glass surfaces followed by evaporation of the solvent at ambient temperature and then dried at 37 °C for 6 h. For comparative purposes, hybrid silica spheres (SIL) were also prepared under identical conditions using the POSS solution.[29] Doxorubicin hydrochloride encapsulated vesicles (POSS-F68-DOX) were obtained when made from solutions containing the drug. A DOX loading of 1 wt % per vesicle was adopted for the present study. Folic acid and DOX conjugated vesicles (POSS-F68-DOX-FOL) were also obtained when made from POSS-F68 solutions containing folic acid and DOX, and the loading of folic acid given was 0.01 wt % of the vesicles. The POSS-F68-DOX and POSS-F68-DOX-FOL were washed with distilled water to remove DOX and FOL freely adsorbed on the outer surface of vesicles and dried at 37 °C for further characterization.

2.3. Characterization. POSS-F68 vesicles were characterized using Fourier transform-infrared spectroscopy (FT-IR), differential scanning calorimetry (DSC), thermogravimetric analysis (TGA), X-ray diffractogram (XRD), scanning electron microscopy (SEM), and high-resolution transmission electron microscopy (HR-TEM). FT-IR measurements were made on Perkin-Elmer spectrum one spectrophotometer in the range of 4000−400 cm^{-1} using KBr pellet containing ca. 2 wt % sample. TGA was performed on a TGA-50 (Shimadzu) thermogravimetric analyzer employing a heating rate of 10 °C/min from 30 to 800 °C under a nitrogen flow of 20 mL/min. DSC analysis was performed using a Perkin-Elmer Pyris 6 differential scanning calorimeter calibrated using indium as standard. XRD data between 2° and 20° 2θ were collected on a Philips X'pert Pro X-ray diffractometer equipped with a graphite monochromator and X'celerator detector. SEM images were taken with a JEOL JSM-5600 LV scanning electron microscope on samples provided with a thin gold coating using a JEOL JFC-1200 fine coater. TEM analysis was performed with an FEI, TECNAI 30G2 S-TWIN microscope with an accelerating voltage of 100 kV. Release characteristics of doxorubicin were studied using a SPEX-Fluorolog F112X spectroflourimeter. For the release experiments, weighed amounts of POSS-F68-DOX-FOL were dispersed in 1 mL of sodium phosphate (PBS) buffer (pH 6.9 and 7.4) in triplicate. The concentration of doxorubicin released was determined by measuring the intensity at an excitation wavelength of 470 nm.

The cytotoxicity of the POSS-F68, POSS-F68-FOL, and POSS-F68-DOX-FOL vesicles was determined *in vitro* by MTT assay using L929 and HeLa cells, and the method is reported elsewhere.[30] The formazan crystals formed were dissolved in DMSO, and absorbance at 570 nm was measured using a plate reader (Finstruments microplate reader). Cells treated with medium were used as the negative control. For drug-uptake studies, HeLa cells were cultured on sterile glass coverslips into 24-well plates, in DMEM medium supplemented with 10% FBS and 1% nonessential amino acids, and allowed to adhere overnight with 5% CO_2 at 37 °C. For evaluating the particle uptake, the cells were incubated with POSS-F68-DOX and POSS-F68-DOX-FOL for 3 h, at concentrations of 0.1 and 0.5 mg/mL. The uptake of the vesicles by cells was imaged using confocal microscope (Nikon A1R), after fixing the cells with 4% paraformaldehyde and staining the nucleus with DAPI nuclear stain. For the flow cytometric evaluation of vesicle endocytosis, HeLa and HOS cells were cultured on T25 culture flasks to 80% confluency. POSS-F68-DOX and POSS-F68-DOX-FOL were suspended in medium without antibiotics and sonicated for 10 min in a water bath. The medium containing the vesicles or the control medium was added to the cells at a concentration of 0.5 mg/mL and incubated for 3 h at 37 °C. The cells were washed thrice with PBS to remove free vesicles, trypsinized, fixed with 4% paraformaldehyde, washed again twice, and resuspended in PBS. The amount of

dx.doi.org/10.1021/la4036997 | *Langmuir* 2014, 30, 340−347

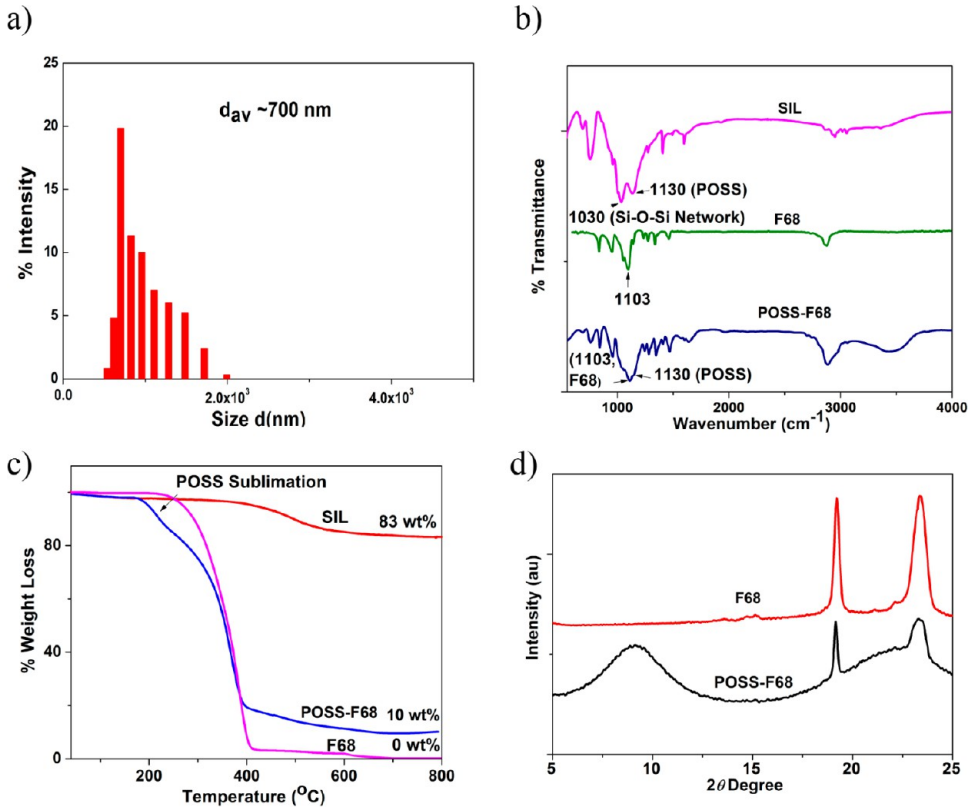

Figure 2. (a) DLS histogram of POSS-F68 vesicles, (b) FT-IR spectra of POSS-F68, F68, and SIL, (c) thermogram of POSS-F68, F68, and SIL, and (d) X-ray diffractogram of POSS-F68 and F68.

endocytosed vesicles was analyzed by a flow cytometer (FACS Aria II, BD Biosciences, U.S.). Cells were identified by forward and side scatter signals, and the percentage of positive cells was calculated by FACS DIVA software (BD Biosciences, U.S.).

3. RESULTS AND DISCUSSION

The POSS solution obtained through the hydrolytic co-condensation of AS and VS in ethanol/water mixture, when diluted with ethanol and mixed with F68, appeared clear and stable. Upon drop-casting and drying the solution, stable spheres were obtained as observed under SEM (Figure 1a). Hollow or vesicular nature of the spheres was confirmed by FM and TEM. Figure 1b shows the fluorescent micrograph of the doxorubicin encapsulated vesicles. Fluorescence was due to doxorubicin adhering uniformly along the inner walls of the dried vesicles and also that dispersed within the wall of the vesicle. The inset of Figure 1b shows vesicles dispersed in PBS, which appeared fully fluorescent due to doxorubicin dispersed uniformly in the aqueous phase filling the inner volume of the vesicles. TEM images (Figure 1c and d) showed contrast difference, which is characteristic of vesicles. The TEM image obtained was that of partially deformed vesicles flattened inward at the center. The high-resolution TEM image of the vesicle (Figure 1e) proved the nanoporous nature of the vesicle wall due to the presence of cage structured POSS. The POSS-F68 vesicles obtained were dispersible in aqueous medium, proving its potential for intravenous injection formulations. Figure 2a shows the DLS histogram of the vesicles. The vesicles showed an average diameter of 700 nm.

It has been known that AS in alcohol−water mixture undergoes hydrolytic co-condensation without an external catalyst, due to the internal catalytic activity of the basic amino group.[31,32] The hydrolyzed siloxane solutions thus obtained from amine containing silanes in alcohol−water mixture have been used for obtaining POSS-intercalated layered aluminosilicates.[32,33] The interlayer spacing of the layered aluminosilicates was increased uniformly through a distance corresponding to the size of the POSS cubes (~1 nm), confirming that the hydrolyzed solution contains completely condensed POSS alone. However, removal of solvents through slow drying of the POSS solution was found to reverse the equilibrium toward incompletely condensed siloxanes resulting in insoluble T-gels.[31] The hydrolytic co-condensation of a mixture of AS and VS in alcohol−water mixture was found to yield heterofunctional POSS having both amino and vinyl groups.[33] On the other hand, hybrid silica spheres (SIL) were formed from the above POSS solution up on solvent-evaporation, through a relatively spontaneous precipitation of fully condensed POSS along with incompletely condensed siloxanes formed during drying of the solvent.[29] In the present study, neutral polymer F68 was included in the POSS solution to allow the spontaneous precipitation of POSS without reversing the equilibrium toward incompletely condensed siloxanes. However, the mixture was found to yield vesicles rather than spheres up on solvent-evaporation. The FT-IR spectra (Figure 2b) of POSS-F68 vesicles showed bands due to vinyl groups 1600 cm^{-1} (C═C_{str}), 1409 cm^{-1} (C−H_{bend}), 3062, and 3025 cm^{-1} (C−H_{str}), aminopropyl groups 1500 cm^{-1} (N−H_{bend}), 2866, and 2932 cm^{-1} (C−H_{str}). The peaks at 1102 and 1243 cm^{-1} correspond to the stretching vibrations of repeating ethylene oxide and propylene oxide units of F68. In the case of SIL, the peaks at 1130 and 1030 cm^{-1} were assigned as due to Si−O−Si_{str}, respectively, from cage-structured POSS and incompletely condensed siloxanes, and the peak at 965 cm^{-1} confirmed the

dx.doi.org/10.1021/la4036997 | Langmuir 2014, 30, 340−347

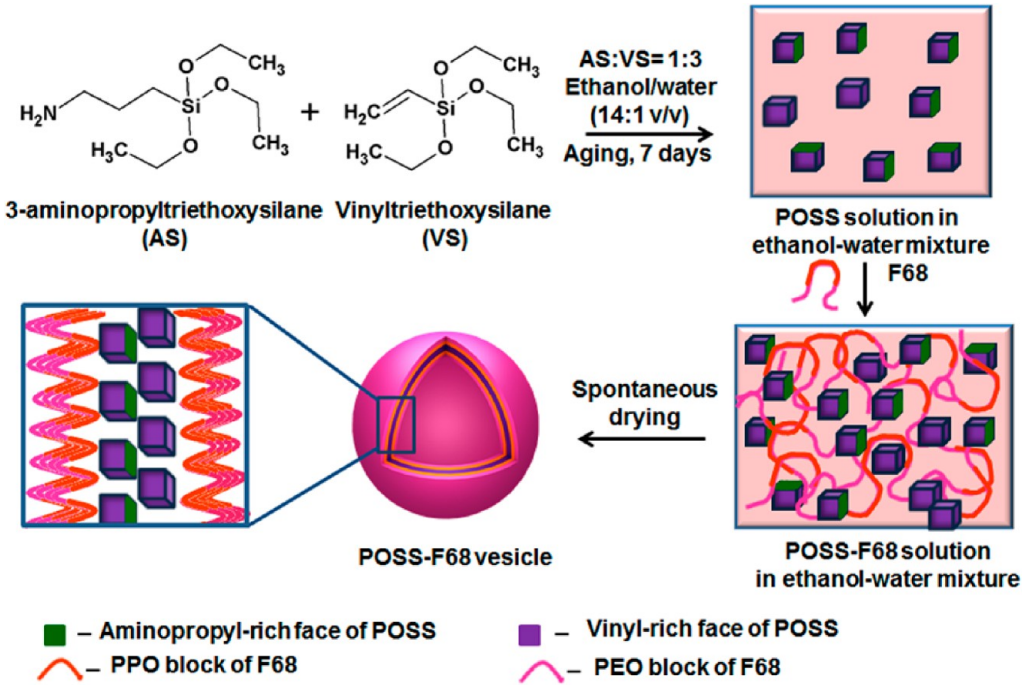

Figure 3. Scheme of formation of POSS-F68 vesicles.

presence of Si−OH from incompletely condensed POSS and siloxane. For POSS-F68, the peak due to fully condensed POSS at 1130 cm^{-1} was not clearly distinguishable as the region was overlapping with the peaks of F68. However, the peak corresponding to incompletely condensed siloxanes at 1030 cm^{-1} was absent, in comparison with SIL. Accordingly, from the FT-IR data, it was confirmed that the POSS-F68 vesicles contain a less significant amount of incompletely condensed siloxane when compared to SIL, which could be due to the spontaneous precipitation of POSS in the presence of F68.

The absence of incompletely condensed siloxanes in POSS-F68 was further confirmed using DSC. In the DSC thermogram (Supporting Information Figure S1), the SIL exhibited an endothermic peak at 126 °C, due to the melting of incompletely condensed siloxanes and the evaporation of adsorbed ethanol.[29] The peak at 126 °C was absent for POSS-F68; instead a strong endothermic peak at 53 °C, corresponding to the melting of F68 alone, was present. Therefore, it can be ascertained that the presence of F68 helps in the effective precipitation POSS, without forming low melting siloxanes and T-gels. Thermogram of POSS-F68 in comparison with SIL and F68 for a temperature range of 40−800 °C is shown in Figure 2c. The SIL showed thermal stability up to 400 °C, with a final char yield of 83 wt % at 800 °C. The high char yield was explained earlier as due to thermal polymerization through the vinyl groups on siloxanes and POSS starting around 200 °C, which prevented sublimation of POSS.[29] F68 was found thermally stable up to 300 °C and decomposed completely without any char yield at a temperature of 700 °C. The POSS-F68 vesicles exhibited a decreased thermal stability with initial significant weight loss starting around 200 °C, and a more distinct weight loss was found at around 270 °C. Because no weight loss was found for F68 and SIL up to 300 °C, the weight loss at around 200−270 °C for POSS-F68 must be due to a component other than F68 and incompletely condensed siloxane, and the weight loss must be due to sublimation of POSS. Because a weight loss amounting 27 wt % due to sublimation of POSS was occurring at around 200−270 °C, it was evident that thermal polymerization through vinyl groups was happening to a lesser extent in POSS-F68, which could be due to the decreased proximity between the vinyl groups. It was ascertained that in POSS-F68, the POSS-bilayers are well-interpenetrated with F68, which decreases intravesicular and completely prevents intervesicular vinyl−vinyl interaction. Thus, the char yield of 10 wt % for POSS-F68 when compared to 83 wt % for SIL was due to increased POSS-sublimation, which in turn proves the presence of fully condensed POSS alone in the vesicles. Figure 2d shows the X-ray diffractograms of POSS-F68 and F68 for a scan angle of 5−25°. The sharp peaks at 19° and 23° 2θ correspond to the structural ordering of F68. In addition to the above peaks, the POSS-F68 showed a peak of low crystallinity at 10 Å. Long-range order arrangement of POSS into hexagonally packed ABCA sequence will result in four strong crystalline peaks in the range of 8−20° where the reflection at around 8° (d-spacing around 10 Å) is caused by size of the POSS.[34] The strongest reflections observed around 8° and 19° were typically exhibited by POSS-polymer nanocomposites, where the POSS formed a bilayer assembly within the polymer matrix.[35] Therefore, through XRD it is confirmed that although the F68 retained its structural ordering in the POSS-F68 vesicles, the peak for POSS at 10 Å indicates only a short-range order of it into a bilayer/two-dimensional arrangement. The reason could be that the presence of F68 might have prevented the POSS cubes from crystallizing beyond a two-dimensional bilayer arrangement. The reflection at about 19° for the POSS-bilayer assembly could not be detected for further confirmation due to the presence of a strong crystalline peak for F68.

A comparison of the size of the POSS-F68 vesicles and SIL spheres for the same dilution of POSS solution using ethanol in a 1:10 ratio revealed a larger size of POSS-F68 vesicles ($d_{av} \approx$ 700 nm) when compared to the SIL spheres ($d_{av} \approx$ 300 nm) (Supporting Information Figure S2). The zeta potential values of SIL and POSS-F68 were −12.7 ± 5.77 and −2.28 ± 1.57

dx.doi.org/10.1021/la4036997 | *Langmuir* 2014, 30, 340−347

mV, respectively. The decreased negative surface charge for the POSS-F68 in comparison with SIL indicated that in POSS-F68 vesicles, neutral F68 is exposed at the surface. Therefore, the plausible mechanism for the formation of POSS-F68 vesicles can be explained as follows. POSS cubes produced through the hydrolytic co-condensation of AS and VS in 1:3 mol ratio possess a greater number of vinyl groups at its corners when compared to 3-aminopropyl groups (Supporting Information Figure S3). However, the nucleophilic hydrolytic co-condensation mechanism will lead to the preferential isolation of hydrophilic amino groups on one face of the POSS cubes when compared to the other faces.[29] Upon spontaneous evaporation of the solvents by drop-casting the POSS-F68 solution in ethanol–water mixture, POSS cubes having lower solubility and an inherent tendency for close packing undergo self-assembly to form bilayers through H-bonding interaction between the 3-aminopropyl-rich faces of the POSS-cubes (Figure 3). With further evaporation of the solvents, the F68 having higher solubility in ethanol–water mixture can stabilize the POSS-bilayers through interaction of its hydrophobic PPO block with vinyl-rich face of POSS-cubes to form extended bilayers, which then closes to form the vesicles. The increase in the size of the POSS-F68 vesicles when compared to SIL could be due to the formation of extended bilayers rather than layer-by-layer self-assembly. The formation mechanism exposes the hydrophilic PEO block of F68 to the outer and inner surfaces of the vesicle wall, which provides it dispersibility in aqueous solvents. The possible reason for the precipitation of POSS into a bilayer without shifting the equilibrium toward incompletely condensed siloxane is the stabilization of POSS in presence of F68. Also, the rate at which self-assembly and formation of vesicle was happening in the presence of F68 could be sufficient to prevent the formation of incompletely condensed network siloxanes and T-gels.

Doxorubicin (DOX) was used as a model drug to evaluate the loading efficiency and controlled release profile of POSS-F68 vesicles, and folic acid (FOL) was used as the targeting ligand. POSS-F68-DOX-FOL (Figure 4) was obtained when

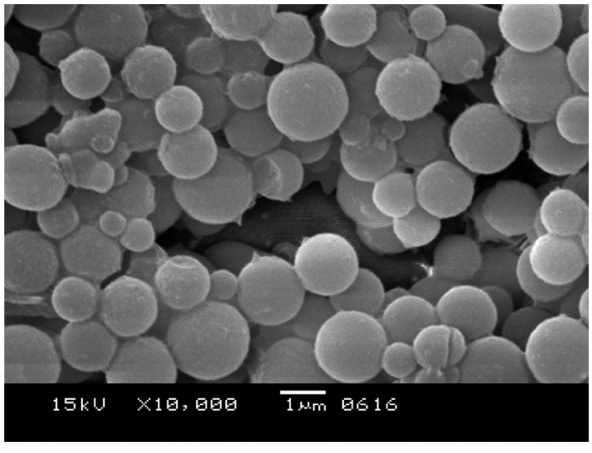

Figure 4. SEM of POSS-F68-DOX-FOL vesicles.

the vesicles were made from POSS solution containing DOX and folic acid. A DOX loading of 1% to the weight of the vesicles was opted for the present study, and an encapsulation efficiency of 85% was obtained. However, a DOX loading capacity up to 5 wt % was confirmed by making the sample in low quantity using a higher drug loading. The encapsulated DOX is expected to be distributed in the inner volume of the vesicles, within the vesicle wall in adsorbed and H-bonded form and also trapped inside of the POSS cubes. A maximum loading of 0.01 wt % was chosen for FOL due to the sparingly soluble nature of folic acid in ethanol–water mixture. The design strategy was based on the assumption that the noncytotoxic FOL when present in excess will not interfere with cancer therapy, but can be H-bonded with the amino-propyl groups present randomly on the exterior surface of the POSS-bilayer. The H-bonded folic acid can get exposed across the F68 layer to the surface of vesicles in the solvated form and provide the required targeting capacity to the vesicles. The presence of folic acid exposed at the surface of the vesicles was proven by a negative zeta-potential value of -18.9 ± 2.3 for POSS-F68-FOL vesicles prepared without DOX. POSS-F68-DOX-FOL has a zeta potential value of -21.2 ± 1.3. The loading efficiency of folate was 78%. The high loading efficiency of DOX and FOL obtained was due to the solvent evaporation technique used for fabricating the vesicles. The *in vitro* release characteristics of doxorubicin were studied in PBS at a body fluid pH of 7.4 and a slightly acidic pH of 6.9, because the extracellular pH values of many cancer tissues are lower than those of normal tissues (Figure 5a). Doxorubicin exhibited a

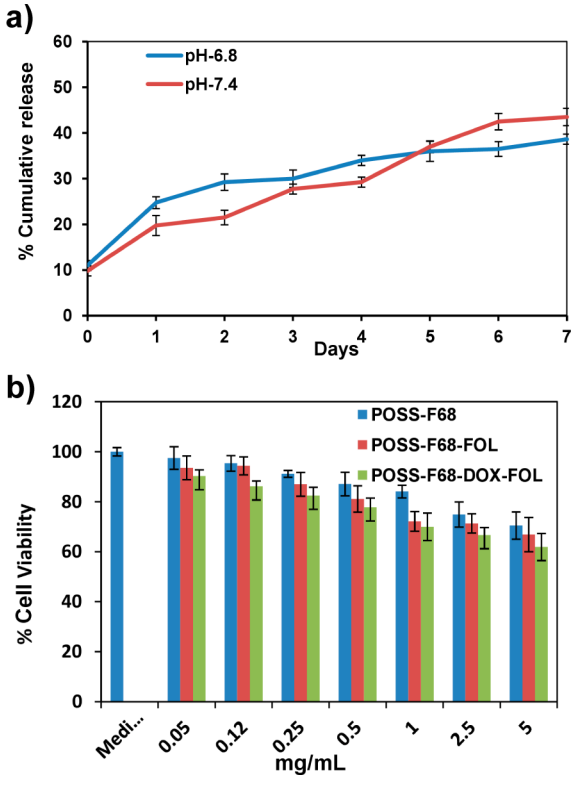

Figure 5. (a) Release profile of doxorubicin from POSS-F68-DOX-FOL into PBS at pH 6.9 and 7.4, and (b) cytotoxicity evaluation of POSS-F68, POSS-F68-FOL, and POSS-F68-DOX-FOL on HeLa cells using MTT-assay.

controlled release profile during 7 days by releasing approximately 40% of the encapsulated drug, and a significant difference in the release pattern at the two pH's was not observed. The vesicles were stable in PBS for 4 days, whereas an increase in the nonvesicle fraction was observed in 7 days due to gradual decomposition of the vesicle bilayer, as supported by optical micrographs (Supporting Information

dx.doi.org/10.1021/la4036997 | *Langmuir* 2014, 30, 340–347

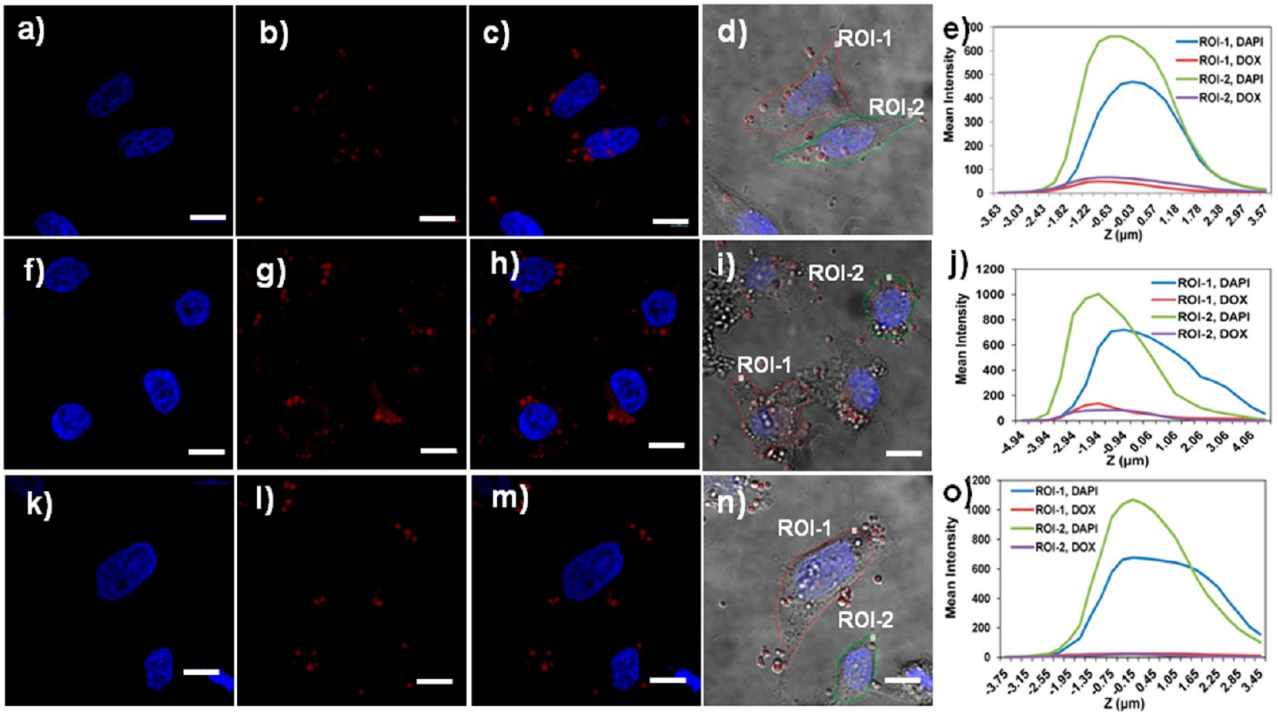

Figure 6. Confocal images of human HeLa cells incubated with POSS-F68-DOX-FOL at a vesicle solution concentration of 0.1 mg/mL (a–d) and 0.5 mg/mL (f–i), and POSS-F68-DOX (0.5 mg/mL) (k–n) for 3 h, and the corresponding quantitative analysis of DAPI and DOX fluorescence for the z-stacks in the region of interest (ROI) highlighted. Each series represents nuclei of cells visualized using DAPI, red fluorescence from DOX, overlay of fluorescence from DAPI and DOX, overlay of the fluorescent images with the DIC image, and the axial quantitative analysis plot. Scale bar represents 10 μm.

Figure S4). These findings indicate that POSS-F68 vesicles are useful for controlled drug delivery applications.

Biocompatibility is a critical factor that should be satisfied by carriers for drug delivery applications. Cytotoxicities of the POSS-F68, POSS-F68-FOL, and POSS-F68-DOX-FOL were investigated *in vitro* by measuring the cell viability of L929 cells and HeLa cells after 24 h incubation with the vesicles, using MTT-assay. POSS-F68, POSS-F68-FOL, and POSS-F68-DOX-FOL gave a cell viability of L929 cells close to 100% up to a concentration of 1 mg mL^{-1} (see Supporting Information Figure S5). However, a concentration-dependent cytotoxicity induction was evident with increasing vesicle concentration. The cell viabilities following exposure of POSS-F68, POSS-F68-FOL, and POSS-F68-DOX-FOL vesicles to L929 cells for 24 h at a vesicle concentration of 5 mg/mL were 71.51 ± 3.10%, 69.88 ± 2.9%, and 64.92 ± 3.12%, respectively. The vesicles exhibited more cytotoxicity on HeLa cells when compared to that on L929 cells, for a given concentration (Figure 5b). The cell viabilities following exposure of POSS-F68, POSS-F68-FOL, and POSS-F68-DOX-FOL vesicles to HeLa cells for 24 h at a vesicle concentration of 5 mg/mL were 70.21 ± 4.14%, 66.54 ± 3.9%, and 61.12 ± 4.11%, respectively. The increased cytotoxicity on HeLa cells when compared to that on L929 cells could be due to the enhanced uptake of folate conjugated vesicles by HeLa cells overexpressing folate receptors. The relatively lower value of cytotoxicity of POSS-F68-DOX-FOL could be due to the low DOX-loading given for the vesicles and slow release rate of the DOX from the vesicles, which is advantageous for intravenous targeted formulations to avoid the loss of drug before reaching the tumor site. The results demonstrate that the POSS-F68 and POSS-F68-FOL vesicles are of low cytotoxicity and have great potential for drug delivery applications.

To further evaluate the potential of the vesicles for drug delivery applications, cellular uptake of POSS-F68-DOX-FOL vesicles was studied using HeLa cells (Figure 6). HeLa cells were incubated with POSS-F68-DOX-FOL (0.1 and 0.5 mg/mL) for 3 h. After incubation, the cells were washed with PBS and fixed. Nuclei of the cells were stained blue using fluorescent dye DAPI, and the uptake was evaluated using confocal microscopy. Figure 6a–e, respectively, shows the nucleus of the HeLa cells stained with DAPI, red fluorescence from DOX, overlay image of fluorescence of DOX and DAPI, overlay of fluorescence with the DIC image of HeLa cells, and the axial quantitative analysis for the z-stacks in the region of interests highlighted, for a vesicle solution concentration of 0.1 mg/mL, and Figure 6f–j shows the same for a solution concentration of 0.5 mg/mL. For the axial quantitative analysis, mean intensity of DAPI and DOX fluorescence for each plane was calculated using NIS Ar software and plotted against *z*-axis distance (low magnification confocal images (Figure S6) and movie of z-stacks are given as Supporting Information). The confocal images and the axial quantitative analysis data showed that the number of POSS-F68-DOX-FOL vesicles endocytosed by the cells was increasing with increase in vesicle solution concentration. To confirm that the uptake of vesicles was folate-receptor mediated, HeLa cells were incubated with POSS-F68-DOX (0.5 mg/mL), and the confocal images and the axial quantitative analysis confirmed that most of the POSS-F68-DOX vesicles were seen outside the cytoplasm (Figure 6k–o) when compared to POSS-F68-DOX-FOL.

The percentage of endocytosis of POSS-F68-DOX-FOL and POSS-F68-DOX by HeLa cells was further evaluated flow-

dx.doi.org/10.1021/la4036997 | *Langmuir* 2014, 30, 340–347

cytometrically as shown in Figure 7, by using a vesicle solution concentration of 0.5 mg/mL. The result has proven that the

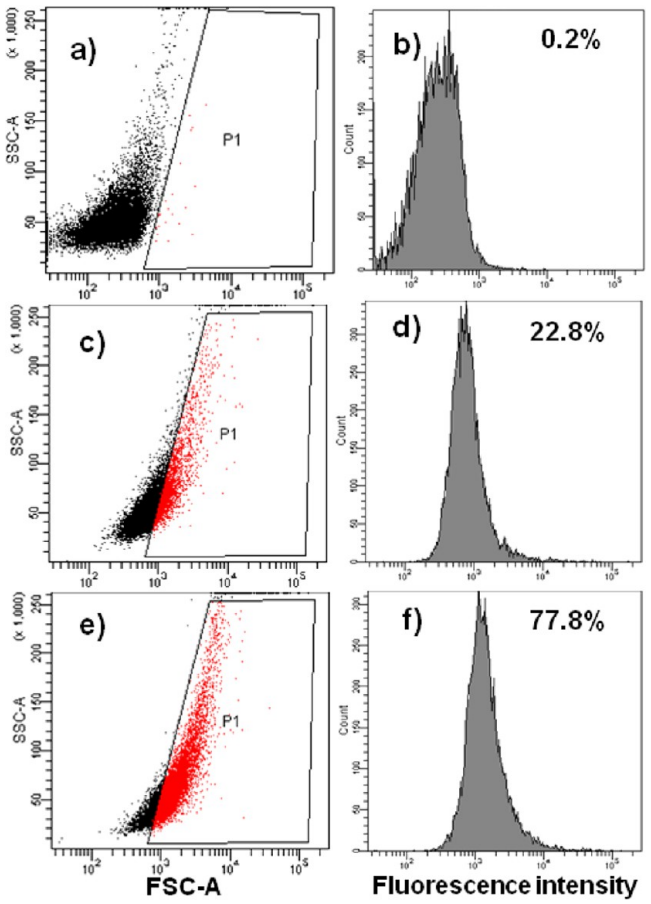

Figure 7. Flow-cytometric analysis of the endocytosis of POSS-F68-DOX (c and d) and POSS-F68-DOX-FOL (e and f) by HeLa cells upon incubation with a vesicle solution concentration of 0.5 mg/mL for 3 h, in comparison with control HeLa cells (a and b).

endocytosis of POSS-F68-DOX-FOL is 50% higher than that of POSS-F68-DOX due to folate receptor mediated cellular uptake. To further prove the folate receptor mediated uptake, POSS-F68-DOX-FOL was incubated with HOS cells, which do not overexpress folate receptors. A lower uptake of POSS-F68-DOX-FOL by HOS cells further confirms that the enhanced uptake of POSS-F68-DOX-FOL by HeLa cells was folate receptor mediated, which in turn indicates a successful folic acid conjugation on the vesicles (Figure 8). The above results demonstrate that the POSS-F68 vesicles in combination with an anti-cancer drug and folic acid are a promising system for targeted anti-cancer therapy. As part of moving toward in vivo evaluation for targeted drug delivery applications, detailed hematological, serum chemistry, and hepatotoxicity analyses of the hybrid vesicles are currently in progress.[36,37]

4. CONCLUSIONS

POSS-F68 vesicles were fabricated through a facile self-assembly and stabilization method. The vesicles have an inner core of POSS bilayer and outer core of F68 in its bilayer arrangement, as revealed by structural evaluations. The vesicles were noncytotoxic, and doxorubicin encapsulated in the vesicles exhibited a controlled release profile in PBS. Uptake of doxorubicin and folate encapsulated vesicles was evaluated

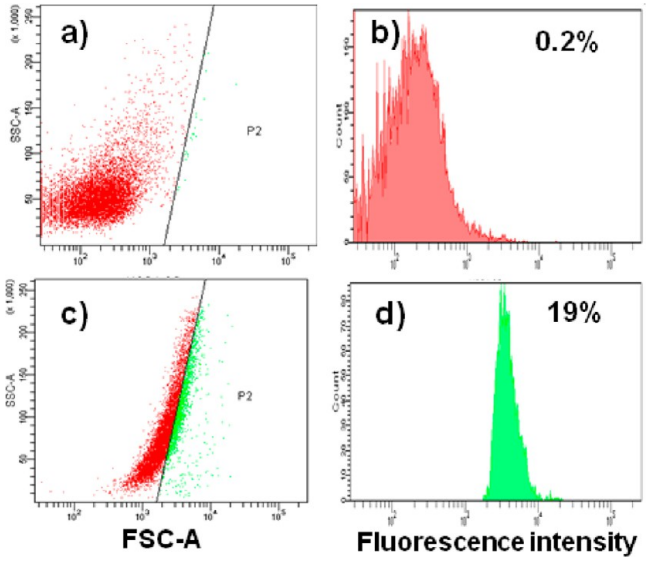

Figure 8. Flow-cytometric analysis of endocytosis of POSS-F68-DOX-FOL (c and d) by HOS cells upon incubation with a vesicle solution concentration of 0.5 mg/mL for 3 h, in comparison with control HOS cells (a and b).

using HeLa cells. Confocal and flow cytometric evaluation proved that POSS-F68 vesicles in combination with folic acid and a chemotherapeutic are potential candidates for targeted intracellular anti-cancer drug delivery.

■ ASSOCIATED CONTENT

Supporting Information

DSC thermogram of POSS-F68, SEM of SIL, possible structures of POSS, optical micrographs proving structural stability of the vesicles, low magnification confocal micrographs, and movie on endocytosis and cytotoxicity evaluation using L929 cells. This material is available free of charge via the Internet at http://pubs.acs.org.

■ AUTHOR INFORMATION

Corresponding Author

*Tel.: +914712520242. Fax: +914712341814. E-mail: pdnair49@gmail.com.

Notes

The authors declare no competing financial interest.

■ ACKNOWLEDGMENTS

This work was supported by INSPIRE-Faculty fellowship and research grant (IFA-CH-19) to B.P.N. from Department of Science and Technology (DST), India. We also thank Director, SCTIMST and Head, BMT wing, SCTIMST for providing the facilities, Dr. Lissy K. Krishnan for flow cytometry, Mr. Willy Paul for DLS and zeta potential measurements, and Dr. Santhosh Kumar T. R. and Mr. Anurup K. G., Rajeev Gandhi Centre for Biotechnology, Trivandrum, for confocal analysis.

■ REFERENCES

(1) Bae, Y. H.; Park, K. Targeted Drug Delivery to Tumors: Myths, Reality and Possibility. *J. Controlled Release* **2011**, *153*, 198−205.

(2) Sailor, M. J.; Park, J.-H. Hybrid Nanoparticles for Detection and Treatment of Cancer. *Adv. Mater.* **2012**, *24*, 3779−3802.

(3) Geng, J.; Li, K.; Pu, K.-Y.; Ding, D.; Liu, B. Conjugated Polymer and Gold Nanoparticle Co-loaded PLGA Nanocomposites with

Eccentric Internal Nanostructure for Dual-modal Targeted Cellular Imaging. *Small* **2012**, *8*, 2421−2429.
(4) Zhang, B.; Li, Y.; Fang, C.-Y.; Chang, C.-C.; Chen, C.-S.; Chen, Y.-Y.; Chang, H.-C. Receptor-mediated Cellular Uptake of Folate-conjugated Fluorescent Nanodiamonds: a Combined Ensemble and Single-particle Study. *Small* **2009**, *5*, 2716−2721.
(5) Wang, H.; Wang, S.; Liao, Z.; Zhao, P.; Su, W.; Niu, R.; Chang, J. Folate-targeting Magnetic Core-shell Nanocarriers for Selective Drug Release and Imaging. *Int. J. Pharm.* **2012**, *430*, 342−349.
(6) Wang, H.; Wu, Y.; Zhao, R.; Nie, G. Engineering the Assemblies of Biomaterial Nanocarriers for Delivery of Multiple Theranostic Agents with Enhanced Antitumor Efficacy. *Adv. Mater.* **2013**, *25*, 1616−1622.
(7) Shen, J.-M.; Guan, X.-M.; Liu, X.-Y.; Lan, J.-F.; Cheng, T.; Zhang, H.-X. Luminescent/Magnetic Hybrid Nanoparticles with Folate-Conjugated Peptide Composites for Tumor-Targeted Drug Delivery. *Bioconjugate Chem.* **2012**, *23*, 1010−1021.
(8) Qiang, X.; Wu, T.; Fan, J.; Wang, J.; Song, F.; Sun, S.; Jiang, J.; Peng, X. Preparation and Folic Acid Conjugation of Fluorescent Polymer Nanoparticles for Cancer Cell Targeting. *J. Mater. Chem.* **2012**, *22*, 16078−16083.
(9) Wang, C.; Li, Z.; Cao, D.; Zhao, Y.; Gaines, J. W.; Bozdemir, O. A.; Ambrogio, M. W.; Frasconi, M.; Botros, Y. Y.; Zink, J. I.; Stoddart, J. F. Stimulated Release of Size Selected Cargos in Succession from Mesoporous Silica Nanoparticles. *Angew. Chem., Int. Ed.* **2012**, *51*, 5460−5465.
(10) Tarn, D.; Xue, M.; Zink, J. I. pH-Responsive Dual Cargo Delivery from Mesoporous Silica Nanoparticles with a Metal-Latched Nanogate. *Inorg. Chem.* **2013**, *52*, 2044−2049.
(11) Rim, H. P.; Min, K. H.; Lee, H. J.; Jeong, S. Y.; Lee, S. C. pH-Tunable Calcium Phosphate Covered Mesoporous Silica Nanocontainers for Intracellular Controlled Release of Guest Drugs. *Angew. Chem., Int. Ed.* **2011**, *50*, 8853−8857.
(12) Gai, S.; Yang, P.; Ma, P.; Wang, D.; Li, C.; Li, X.; Niu, N.; Lin, J. Fibrous-structured Magnetic and Mesoporous Fe3O4/silica Microspheres: Synthesis and Intracellular Doxorubicin Delivery. *J. Mater. Chem.* **2011**, *21*, 16420−16426.
(13) Ferris, D. P.; Lu, J.; Gothard, C.; Yanes, R.; Thomas, C. R.; Olsen, J.-C.; Stoddart, J. F.; Tamanoi, F.; Zink, J. I. Synthesis of Biomolecule-Modified Mesoporous Silica Nanoparticles for Targeted Hydrophobic Drug Delivery to Cancer Cells. *Small* **2011**, *7*, 1816−1826.
(14) Pan, L.; He, Q.; Liu, J.; Chen, Y.; Ma, M.; Zhang, L.; Shi, J. Nuclear-Targeted Drug Delivery of TAT Peptide-Conjugated Monodisperse Mesoporous Silica Nanoparticles. *J. Am. Chem. Soc.* **2012**, *134*, 5722−5725.
(15) Tan, H.; Wang, M.; Yang, C. T.; Pant, S.; Bhakoo, K. K.; Wong, S. Y.; Chen, Z. K.; Li, X.; Wang, J. Silica Nanocapsules of Fluorescent Conjugated Polymers and Superparamagnetic Nanocrystals for Dual-Mode Cellular Imaging. *Chem.—Eur. J.* **2011**, *17*, 6696−6706.
(16) Tan, H.; Zhang, Y.; Wang, M.; Zhang, Z.; Zhang, X.; Yong, A. M.; Wong, S. Y.; Chang, A. Y.; Chen, Z.-K.; Li, X.; Choolani, M.; Wang, J. Silica-shell Cross-linked Micelles Encapsulating Fluorescent Conjugated Polymers for Targeted Cellular Imaging. *Biomaterials* **2012**, *33*, 237−246.
(17) Zhang, Y.; Wang, M.; Zheng, Y.; Tan, H.; Hsu, B. Y.; Yang, Z.; Wong, S. Y.; Chang, A. Y.; Choolani, M.; Li, X.; Wang, J. PEOlated Micelle/Silica as Dual-Layer Protection of Quantum Dots for table and Targeted Bioimaging. *Chem. Mater.* **2013**, *25*, 2976−2985.
(18) Harrington, K. J.; Lewanski, C. R.; Stewart, J. S. Liposomes as Vehicles for Targeted Therapy of Cancer. Part 2: Clinical Development. *Clin. Oncol. Cancer Res.* **2000**, *12*, 16−24.
(19) Yuan, H.; Luo, K.; Lai, Y.; Pu, Y.; He, B.; Wang, G.; Wu, Y.; Gu, Z. A Novel Poly(l-glutamic acid) Dendrimer Based Drug Delivery System with Both pH-Sensitive and Targeting Functions. *Mol. Pharmaceutics* **2010**, *7*, 953−962.
(20) McCusker, C.; Carroll, J. B.; Rotello, V. M. Cationic Polyhedral Oligomeric Silsesquioxane(POSS) Units as Carriers for Drug Delivery Processes. *Chem. Commun.* **2005**, 996−998.
(21) Ghanbari, H.; Cousins, B. G.; Seifalian, A. M. A Nanocage for Nanomedicine: Polyhedral Oligomeric Silsesquioxane(POSS). *Macromol. Rapid Commun.* **2011**, *32*, 1032−1046.
(22) Wang, Z.; Li, Y.; Dong, X.-H.; Yu, X.; Guo, K.; Su, H.; Yue, K.; Wesdemiotis, C.; Cheng, S. Z. D.; Zhang, W.-B. Giant Gemini Surfactants Based on Polystyrene−hydrophilic Polyhedral Oligomeric Silsesquioxane Shape Amphiphiles: Sequential "click" Chemistry and Solution Self-assembly. *Chem. Sci.* **2013**, *4*, 1345.
(23) Yu, X.; Zhong, S.; Li, X.; Tu, Y.; Yang, S.; Van Horn, R. M.; Ni, C.; Pochan, D. J.; Quirk, R. P.; Wesdemiotis, C.; et al. A Giant Surfactant of Polystyrene-(carboxylic Acid-functionalized Polyhedral Oligomeric Silsesquioxane) Amphiphile with Highly Stretched Polystyrene Tails in Micellar Assemblies. *J. Am. Chem. Soc.* **2010**, *132*, 16741−16744.
(24) Yang, C.; Deng, Y.; Zeng, B.; Yuan, C.; Chen, M.; Luo, W.; Liu, J.; Xu, Y.; Dai, L. Hybrid Amphiphilic Block Copolymers Containing Polyhedral Oligomeric Silsesquioxane: Synthesis, Characterization, and Self-assembly in Solutions. *J. Polym. Sci., Part A: Polym. Chem.* **2012**, *50*, 4300−4310.
(25) Shih, R.-S.; Lu, C.-H.; Kuo, S.-W.; Chang, F.-C. Hydrogen Bond-Mediated Self-Assembly of Polyhedral Oligomeric Silsesquioxane-Based Supramolecules. *J. Phys. Chem. C* **2010**, *114*, 12855−12862.
(26) Yu, B.; Jiang, X.; Qin, N.; Yin, J. Thiol−ene Photocrosslinked Hybrid Vesicles from Co-assembly of POSS and Poly(ether Amine)-(PEA). *Chem. Commun.* **2011**, *47*, 12110.
(27) Liu, D.; Yu, B.; Jiang, X.; Yin, J. Responsive Hybrid Microcapsules by the One-Step Interfacial Thiol−Ene Photopolymerization. *Langmuir* **2013**, *29*, 5307−5314.
(28) Kabanov, A. V.; Batrakova, E. V.; Alakhov, V. Y. Pluronic Block Copolymers for Overcoming Drug Resistance in Cancer. *Adv. Drug Delivery Rev.* **2002**, *54*, 759−779.
(29) Nair, B. P.; Pavithran, C. Bifunctionalized Hybrid Silica Spheres by Hydrolytic Cocondensation of 3-aminopropyltriethoxysilane and Vinyltriethoxysilane. *Langmuir* **2010**, *26*, 730−735.
(30) Nair, B. P.; Sharma, C. P. Poly(lactide-*Co*-glycolide)−Laponite−F68 Nanocomposite Vesicles through a Single-Step Double-Emulsion Method for the Controlled Release of Doxorubicin. *Langmuir* **2012**, *28*, 4559−4564.
(31) Feher, F. J.; Wyndham, K. D. Amine and Ester-substituted Silsesquioxanes: Synthesis, Characterization and Use as a Core for Starburst Dendrimers. *Chem. Commun.* **1998**, 323−324.
(32) Szabó, *α*.; Gournis, D.; Karakassides, M. A.; Petridis, D. Clay−Aminopropylsiloxane Compositions. *Chem. Mater.* **1998**, *10*, 639−645.
(33) Nair, B. P.; Pavithran, C.; Sudha, J. D.; Prasad, V. S. Microvesicles through Self-Assembly of Polystyrene−Clay Nanocomposite. *Langmuir* **2010**, *26*, 1431−1434.
(34) Zheng, L.; Waddon, A. J.; Farris, R. J.; Coughlin, E. B. X-ray Characterizations of Polyethylene Polyhedral Oligomeric Silsesquioxane Copolymers. *Macromolecules* **2002**, *35*, 2375−2379.
(35) Waddon, A. J.; Coughlin, E. B. Crystal Structure of Polyhedral Oligomeric Silsequioxane(POSS) Nano-materials: A Study by X-ray Diffraction and Electron Microscopy. *Chem. Mater.* **2003**, *15*, 4555−4561.
(36) Moore, L.; Chow, E. K.; Osawa, E.; Bishop, J. M.; Ho, D. Diamond-lipid Hybrids Enhance Chemotherapeutic Tolerance and Mediate Tumor Regression. *Adv. Mater.* **2013**, *25*, 3532−3541.
(37) Mulvey, J. J.; Villa, C. H.; McDevitt, M. R.; Escorcia, F. E.; Casey, E.; Scheinberg, D. A. Self-assembly of Carbon Nanotubes and Antibodies on Tumours for Targeted Amplified Delivery. *Nat. Nanotechnol.* **2013**, *8*, 763−771.